# A novel wiring scheme for standard chips enabling high-accuracy impedance cytometry

Federica Caselli [a,*], Adele De Ninno [a], Riccardo Reale [a], Luca Businaro [b], Paolo Bisegna [a,*]

[a] Department of Civil Engineering and Computer Science, University of Rome Tor Vergata, 00133 Rome, Italy
[b] Institute for Photonics and Nanotechnologies, Italian National Research Council, 00156 Rome, Italy

## ABSTRACT

While there is a great interest in microfluidic impedance cytometry as a label-free approach for single-particle analysis, the accuracy of the technique is challenged by the positional dependence issue, i.e. identical particles flowing in the microchannel along different trajectories provide different signals. We solve this issue without resorting to particle focusing, by means of a straightforward modification of the conventional wiring scheme for the standard impedance chip comprising two pairs of facing electrodes. Instead of applying the AC voltage to electrodes on the same side of the channel and collecting the differential current flowing through the electrodes on the other side, we apply the AC voltage to diagonally opposite electrodes and collect the differential current flowing through the remaining ones. Therefore, the bipolar signal recorded upon the passage of a particle shows opposite pulses with *different* amplitude. The relative difference of the latter is a new metric enabling a simple compensation procedure of the signal impedance for off-center particles. Impedance data for 5.2, 6, and 7 μm particles are collected, and coefficients of variation in (electrical) diameter of particles respectively of 2.8%, 1%, and 1.2%, similar to the manufacturers' quoted values, are obtained. The novel operation mode is successfully implemented also in a coplanar electrode configuration, exploiting two pairs of liquid electrodes.

© 2017 The Author(s). Published by Elsevier B.V. This is an open access article under the CC BY-NC-ND license (http://creativecommons.org/licenses/by-nc-nd/4.0/).

## 1. Introduction

Microfluidic impedance cytometry is a non-invasive technique for the electrical characterization of single particles and cells [1,2]. Compared with traditional approaches like flow cytometry, its main advantages are the label-free nature, requiring minimal sample processing, and the potential for low-cost and portable implementation. The basic principle is as follows: (i) an AC electric field is established in a microchannel equipped with microelectrodes and filled with a conductive fluid; (ii) the field perturbation induced by the passage of a flowing particle is measured as an electric current signal; (iii) the latter is processed to extract valuable information for particle characterization. As an example, information on size, membrane capacitance, and cytoplasm conductivity of biological cells can be obtained depending on the frequency of the AC electric field (e.g., [3–7]).

The rapid progress in microfabrication technologies over the past two decades has fostered the development of microfluidic impedance cytometry. Two main types of electrode configuration have been proposed in the literature [1]: either channels with coplanar electrodes embedded in one side of the channel, or channels with parallel facing electrodes embedded in opposite sides. The former configuration enjoys easiness of fabrication, whereas the latter generally has higher sensitivity. A common design includes two pairs of facing electrodes used in a differential measuring scheme. It is employed in both research prototypes (e.g., [8–12]) and commercial products (e.g., Micronit EIS chips, Amphasys microflow cytometer).

Unfortunately, the resolution and accuracy of both coplanar and facing electrode configurations is challenged by the positional dependence of the measured signals, i.e. identical particles flowing along different trajectories in the microchannel provide different signals. This is due to the non-uniformity of the electric field in the sensing region [13–16], and produces blurring of estimated particle properties.

An approach to cope with the positional dependence of the measured traces is particle focusing, for example by means of hydrodynamic effects (like sheath flow [17] or inertial focusing

* Corresponding authors.
  *E-mail addresses:* caselli@ing.uniroma2.it (F. Caselli), bisegna@uniroma2.it (P. Bisegna).
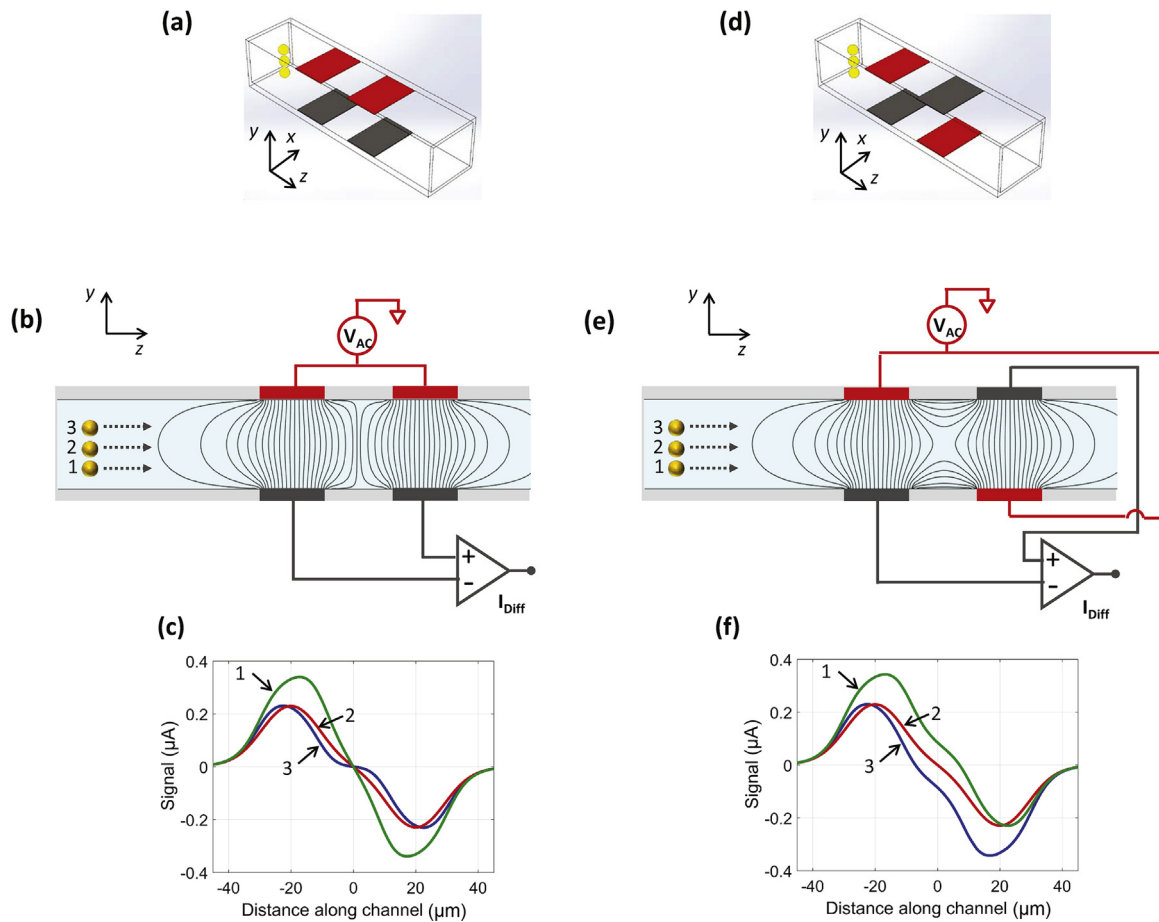
**Fig. 1.** Facing electrode chip. (a)–(c) Conventional operation mode. (a) 3D view and (b) side view cartoon. An AC voltage is applied to the top stimulating electrodes and the differential current flowing through the bottom measuring electrodes is collected. Typical current lines are shown. (c) Differential signals (real part, simulation results) produced by an insulating particle passing through the sensing region along three different trajectories: close to the bottom of the channel (curve 1), through the middle of the channel (curve 2) and close to the top of the channel (curve 3). Each curve consists of a pair of opposite Gaussian pulses with the same amplitude. (d)–(f) Proposed operation mode. (d) 3D view and (e) side view cartoon. An AC voltage is applied to diagonally opposite stimulating electrodes and the differential current flowing through the remaining measuring electrodes is collected. (f) Differential signals relevant to the three different trajectories considered in panel (c) (real part, simulation results). Each curve consists of a pair of opposite Gaussian pulses with different amplitude. Pulse amplitude difference depends on particle trajectory height.

[18]) or active focusing mechanisms (e.g., dielectrophoresis [19,20] and acustophoresis [21]). However, they increase the complexity of the system and may be difficult to optimize for a heterogeneous sample.

Two effective strategies not requiring focusing systems have been recently proposed to overcome the positional dependence issue [22,23]. Both methods introduce a new metric related to particle trajectory height, used as a pivotal tool to compensate for the spread in signal amplitude by means of simple calibration. One metric is the ratio between the peak-to-peak times of two differential current signals, relevant to current paths with different spatial orientation, provided by a measurement scheme involving five pairs of facing electrodes [22]. Another metric is the "relative prominence" of the bipolar double-Gaussian-shaped traces recorded using a configuration involving five coplanar electrodes [23]. Multielectrode configurations provide unique signatures [24], however they require a larger sensing volume, thus increasing the number of coincidences for a given sample concentration [25].

In this work we show that it is possible to obtain high-accuracy impedance data using the standard chip design comprising two pairs of facing electrodes. This is achieved by a straightforward modification of the wiring scheme with respect to the classic operation mode. The approach is also implemented in a coplanar electrode configuration using two pairs of liquid electrodes. The key concept of the proposed modality is presented and discussed in

Section 2, and the experimental validation is presented in Sections 3–4.

## 2. Operating principle

The conventional operation mode of the standard impedance chip comprising two pairs of facing electrodes is depicted in Fig. 1(a) and (b): an AC voltage is applied to the top stimulating electrodes, and the differential current flowing through the bottom measuring electrodes is collected. The passage of a particle is detected as two opposite pulses with the same amplitude [14,27], respectively recorded when the particle is between the left or right pair of electrodes (Fig. 1(c), simulation results[1]). Pulse amplitude primarily depends on the change in the transversal current (i.e., current flowing through a measuring electrode originating from the opposite stimulating one) upon the passage of a particle. Pulse amplitude at low frequency is therefore a measure of particle volume [3,2]. However, the electric field within the sensing region is non-uniform due to fringing effects [13,15]. Hence, pulse amplitude also depends on particle trajectory height, i.e. $y$-coordinate of particle center (Fig. 1(c)). A further contribution to pulse amplitude comes from

---

[1] Details of finite element model equations have been described elsewhere [28,29].
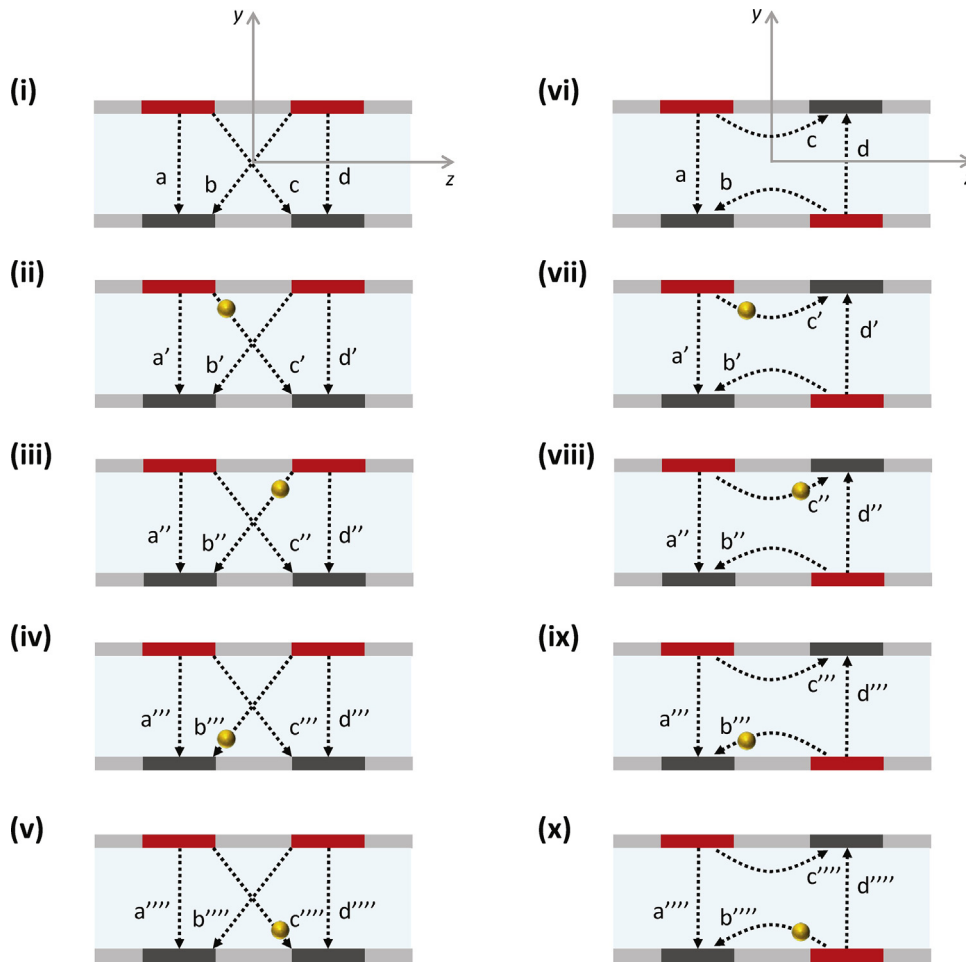
**Fig. 2.** Diagrams of the current paths between the four electrodes in the impedance chip, using (i)–(v) conventional or (vi)–(x) new wiring, as provided by a simple equivalent circuit. In (i), (vi) there is no particle and the current paths are symmetrical; the transversal currents, $a$ and $d$, are equal, and so are the cross currents, $b$ and $c$. Therefore, the differential current $I_{diff} = (d + c) - (a + b) = (d - a) + (c - b)$ vanishes. A particle flowing along a trajectory in the upper half of the channel is considered in (ii), (iii), and (vii), (viii), whereas a particle flowing along a mirrored trajectory about the channel axis $z$ is considered in (iv), (v), and (ix), (x). For both trajectories, two particle locations are considered, mirrored along the center line $y$ between the two pairs of electrodes. By symmetry arguments, it follows that the transversal currents satisfy the relationships: $a' = d'' = a''' = d''''$, $d' = a'' = d''' = a''''$, whereas the cross currents satisfy the relationships (ii)–(v) $b' = c'' = c''' = b''''$, $c' = b'' = b''' = c''''$ when the conventional wiring is used, or the relationships (vii)–(x) $b' = b'' = c''' = c''''$, $c' = c'' = b''' = b''''$ when the new wiring is used. Using the relation $I'_{diff} = (d' - a') + (c' - b')$ and the analogous relations for $I''_{diff}, I'''_{diff}, I''''_{diff}$, it turns out that (ii)–(iii) $I'_{diff} = -I''_{diff}$, and (iv)–(v) $I'''_{diff} = -I''''_{diff}$, when the conventional wiring is used. Therefore, left- and right-pulse amplitudes are equal and convey the same information. Moreover, observing that $b' > c'$, it follows that (ii), (iv) $I'_{diff} < I'''_{diff}$, and the well-known top-bottom asymmetry prevails [14] (Fig. 1(c), curves 1 and 3). On the other hand, when the new wiring is used, it turns out that (vii), (x) $I'_{diff} = -I''''_{diff}$, and (viii), (ix) $I''_{diff} = -I'''_{diff}$, amounting to center symmetry of the system (Fig. 1(f), curves 1 and 3). If the particle flows along a trajectory in the upper half of the channel, (vii) $I'_{diff} = (d' - a') + (c' - b')$ and (viii) $I''_{diff} = (d'' - a'') + (c'' - b'') = -(d' - a') + (c' - b')$ are not opposite quantities: the system is asymmetric left to right. However, both $I'_{diff}$ and $I''_{diff}$ are available and measured, therefore the transversal contribution $(d' - a')$ and the cross contribution $(c' - b')$ to the differential current can be separately estimated by respectively averaging and subtracting $I'_{diff}$ and $I''_{diff}$. Analogous information is obtained (ix), (x) from $I'''_{diff}$ and $I''''_{diff}$ if the particle flows in the lower half of the channel. The transversal contribution to the differential current conveys information on particle volume, with top-bottom and left–right symmetry (i.e., $(d' - a') = -(d'' - a'') = (d''' - a''') = -(d'''' - a'''')$). That quantity mildly depends on particle trajectory height, due to fringing of the electric field. The cross contribution to the differential current has opposite sign if the particle travels (vii), (viii) in the upper half or (ix), (x) in the lower half of the channel (i.e., $(c' - b') = (c'' - b'') = -(c''' - b''') = -(c'''' - b'''')$). That quantity is a new metric related to particle trajectory height, useful to solve the positional dependence issue.

the cross current between the left and right pair of electrodes (i.e., current flowing through a measuring electrode originating from the diagonally opposite stimulating one). As a consequence of the cross current, pulse amplitude is higher when the particle flows closer to the measuring electrodes than to the stimulating ones (the system is asymmetric top to bottom) [14].

The proposed operation mode is depicted in Fig. 1(d) and (e): an AC voltage is applied to diagonally opposite stimulating electrodes and the differential current flowing through the remaining measuring electrodes is collected. This simple modification is suggested by the following heuristic observation. A particle flowing in the lower half of the channel (Fig. 1(e), trajectory 1) is located closer to the bottom measuring electrode than to the top stimulating one when detected by the left pair of electrodes. Then, it is located far-

ther to the top measuring electrode than to the bottom stimulating one when detected by the right pair of electrodes. Accordingly, the left pulse of the recorded signal is expected to have higher amplitude than the right pulse, as confirmed by numerical simulations (Fig. 1(f), curve 1). The opposite behavior is expected for particles flowing in the upper half of the channel (Fig. 1(f), curve 3), whereas particles traveling through the middle of the channel yield pulses with equal amplitude (Fig. 1(f), curve 2). This suggests that pulse amplitude difference is related to particle trajectory height, thus lending itself as a metric useful to treat the positional dependence issue (cf. also the simulation results reported in [30]).

The current paths established in the sensing region upon the passage of a flowing particle, when either conventional or new wiring scheme is used, are compared in Fig. 2 using a simple equiva-
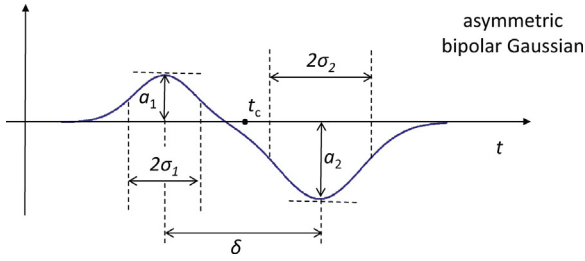
**Fig. 3.** Asymmetric bipolar Gaussian template used to fit the experimental traces collected using the proposed wiring scheme.

lent circuit. It is shown that pulse amplitude difference, amounting to left–right asymmetry inherent to the new wiring scheme, is caused by cross currents, with a similar mechanism known to cause top-bottom asymmetry inherent to the conventional wiring scheme [14]. However, whereas top-bottom asymmetry is an unwanted effect [22], left–right asymmetry is indeed an asset, because particle trajectories are parallel to the channel axis, so that both left- and right-pulse amplitudes are available and measured during the particle flow. These two independent quantities allows one to separate the transversal and cross current contributions embedded in the recorded pulses, by respectively averaging and subtracting the left- and right-pulse amplitudes (Fig. 2). Pulse amplitude average, i.e. transversal current contribution, is a measure of particle volume (at low frequency), only suffering from mild positional dependence due to fringing of the electric field, and its cube root is proportional to particle diameter. Pulse amplitude difference, unveiling cross current contribution, conveys information on particle trajectory height (e.g., it has opposite sign if the particle flows in the upper or lower half of the channel). In fact, the relative difference of pulse amplitudes (i.e., pulse amplitude difference divided by pulse amplitude average) is here chosen, in order to obtain a metric independent of particle size.

An asymmetric bipolar Gaussian template (Fig. 3) can be conveniently fitted to signal traces (Fig. 1(f)) in order to extract the left- and right-pulse amplitudes. The template is obtained as the difference of two shifted Gaussian pulses with different amplitude and width, as follows:

$$s(t) = g_1(t - t_c + \delta/2) - g_2(t - t_c - \delta/2), \tag{1}$$

with

$$g_1(t) = a_1 e^{-t^2/(2\sigma_1^2)}, \; g_2(t) = a_2 e^{-t^2/(2\sigma_2^2)}. \tag{2}$$

It depends on the following parameters: central time moment, $t_c$; transit time, $\delta$; pulse width controls, $\sigma_1$ and $\sigma_2$; pulse amplitude controls, $a_1$ and $a_2$.

According to the previous discussion, an estimate $D$ of the particle diameter $d$ is supplied by the cube root of the mean value of the pulse amplitude controls, $(a_1 + a_2)/2$:

$$D = G \left[ \frac{a_1 + a_2}{2} \right]^{1/3}, \tag{3}$$

where $G$ is a gain factor to account for the electronic circuitry (cf. Supplementary data, Section 1). The estimate $D$ is referred to as "electrical diameter". In addition, the pulse amplitude relative difference, $\Delta$ is introduced:

$$\Delta = \frac{a_2 - a_1}{(a_1 + a_2)/2}. \tag{4}$$

It is shown in Sections 3 and 4 that this new metric enables a simple compensation procedure of the signal impedance for off-center particles, thus solving the positional dependence issue.

By comparison, in the conventional operation mode a symmetric bipolar Gaussian template is used to fit the data, i.e., $a_1 = a_2 = a$

and $\sigma_1 = \sigma_2 = \sigma$ are enforced in Eq. (1). The electrical diameter $D$ is estimated by means of Eq. (3), whereas the pulse amplitude relative difference $\Delta$ is not available (in fact, it vanishes identically).

Using either wiring scheme, the transit time, $\delta$ is available. It is used experimentally to estimate the particle velocity through the system [31,22]:

$$V = \frac{L}{\delta}, \tag{5}$$

referred to as "electrical velocity", where $L$ is the peak-to-peak distance of signal traces (Fig. 1(c), (f)), approximated by the center-to-center spacing of the electrodes. Comparing the simulation traces in Fig. 1(f) with those in Fig. 1(c), it appears that the peak-to-peak distance of traces provided by the new wiring scheme is less sensitive to particle trajectory than the one provided by the conventional wiring scheme.

The proposed operation mode can be straightforwardly implemented also in a coplanar electrode configuration exploiting "liquid electrodes" [26] (Fig. 4(a), (c)). The latter are generated by recessed electrodes patterned at the bottom of dead-end chambers positioned perpendicularly to the main channel. They provide a nearly homogeneous electric field over the total channel height while keeping a simple process flow with a single planar metal layer [32,33]. However, the recorded signal traces depend on the lateral position (i.e., $x$-coordinate) of the particle trajectory. Hence, also that layout suffers from the positional dependence issue. Fig. 4 shows a schematic representation of the conventional and new wiring scheme for a coplanar electrode chip comprising two pairs of liquid electrodes. Differential signal traces are similar to the corresponding ones of the facing electrode chip (Fig. 1(c) and (f)) and are accordingly fitted to the Gaussian template in Eq. (1). As in the previous case, electrical diameter $D$, pulse amplitude relative difference $\Delta$, and electrical velocity $V$ are respectively defined in Eqs. (3)–(5).

## 3. Experimental

### 3.1. Microfluidic impedance chips

#### 3.1.1. Facing electrode chip

As a typical facing electrode chip (Fig. 1), a commercial microfluidic chip for electrical impedance spectroscopy of single cells was used (EIS chip, Micronit). The chip is made of borosilicate glass and an inert interstitial layer of dry film resist. It has a straight through channel 28 μm deep and 30 μm wide. There are two sets of double electrodes (Pt). Electrode dimension along channel axis is 20 μm, with planar separation of 20 μm and 28 μm depth separation as based on channel depth. A commercial chip holder was used (Fluidic Connect PRO, Micronit).

#### 3.1.2. Coplanar electrode chip

The chip with coplanar electrode configuration (Fig. 4) is made of a polydimethylsiloxane (PDMS) block containing the microfluidic channel, bonded to a glass slide with deposited Ti/Au microelectrodes (20 nm/200 nm). The PDMS microchannels were replica molded from photolithographically patterned SU-8 molds, while the electrodes were deposited on glass using optical lithography, e-beam evaporation and lift off procedures. Relevant dimensions are as follows: the main channel is 40 μm wide and 21.5 μm high; lateral channels are 30 μm wide and 30 μm apart from each other; the electrodes in the lateral channels have a 20 μm recess with respect to the main channel. A custom chip holder was used for fluidic and electrical connections.
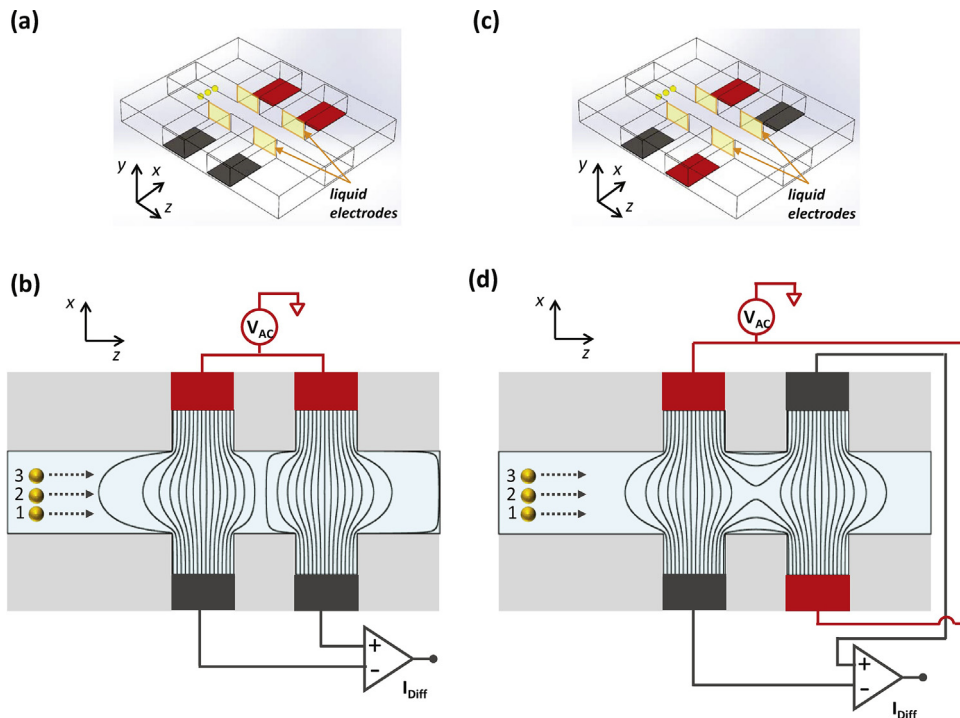
**Fig. 4.** Coplanar electrode chip. Two pairs of liquid electrodes [26] are generated by metal electrodes placed on the floor of two lateral channels. (a and b) Conventional operation mode. An AC voltage is applied to the stimulating electrodes on the same side of the channel axis and the differential current flowing through the measuring electrodes on the other side is collected. (c and d) Proposed operation mode. An AC voltage is applied to diagonally opposite stimulating electrodes and the differential current flowing through the remaining measuring electrodes is collected. A particle passing through the sensing region along trajectories with three different horizontal positions (i.e., at different $x$-coordinate values) is visualized.

### 3.2. Sample preparation

The proposed method is validated by means of polystyrene beads (Sigma–Aldrich and Polysciences). Beads with diameters of 5.2, 6, and 7 μm were suspended in PBS (Phosphate-Buffered Saline) with 0.1% Tween 20 to avoid bead aggregation, and sufficient sucrose to match the density of the beads (1.05 g/cm³). Sample concentration and conductivity were approximately 1000 beads/μl and 1.1 S/m, respectively. The beads were sonicated prior to experiments in order to reduce cluster formation.

### 3.3. Data acquisition and processing

A syringe pump (Harvard Apparatus) operating at 10 μl/min was used for fluidic control. Electrical measurements were performed using an impedance spectroscope (HF2IS, Zurich Instruments, 14 bit A/D conversion at 210 M sample per second), along with a transimpedance amplifier (HF2TA, Zurich Instruments) for signal conditioning. A signal of 4 V [respectively, 8 V] at 0.5 MHz was applied to the stimulating electrodes of the facing electrode chip [respectively, of the coplanar electrode chip] and the differential current flowing through the virtual-ground measuring electrodes was demodulated and recorded (readout rate 115 k sample per second, 20 kHz filter bandwidth). Pulse amplitude average of typical events (i.e., signals generated by the passage of a particle in the sensing region) was in the range (0.15, 0.55) μA [respectively, (0.04, 0.20) μA] depending on particle size and trajectory, whereas the standard deviation of noise was around 4 nA for both electrode configurations.

The following experiments were carried out. The facing electrode chip was used first. Four samples were analyzed, relevant to the three populations of beads and a mixture of them. For each sample, two measurements were acquired (approximately 50,000 beads for each population, 150,000 beads for the mixture), using the conventional wiring (Fig. 1(b)) or the proposed wiring (Fig. 1(e)). The same sequence was repeated using the coplanar electrode chip (Fig. 4(b) or (d)).

Collected data streams were processed using a custom Matlab script. Segmentation was first carried out, aimed at extracting events from the data stream. For each detected event, feature extraction was then performed by fitting the asymmetric bipolar Gaussian template (Eq. (1)) to the recorded trace, thus obtaining the relevant parameters $t_c$, $\delta$, $\sigma_1$, $\sigma_2$, $a_1$, and $a_2$. The histogram of the root mean squared error of the fit, normalized by the mean value of the pulse amplitude control, $(a_1 + a_2)/2$, is reported in Supplementary data, Figure S1. Data collected using the conventional wiring were processed by means of the classic symmetric bipolar Gaussian template.

## 4. Results

Fig. 5 shows a density plot for 6 μm diameter beads, with the pulse amplitude relative difference $\Delta$ (Eq. (4)) plotted against the electrical diameter $D$ (Eq. (3)), as measured using the proposed wiring scheme. Examples of experimental single particle signals are shown in panels (i)–(vii), along with arrows indicating the position of the particle on the density plot. The difference in the amplitudes of the two opposite pulses predicted in simulation (Fig. 1(f)) and explained by the simple equivalent circuit in Fig. 2 is experimentally confirmed. In addition to the experimental signals, their fitting templates are also shown in panels (i)–(vii), showing excellent accuracy. It is pointed out that such a density plot is unavailable using the conventional wiring scheme. In fact the latter yields equal pulse amplitudes, thus ruling out the information content of the metric $\Delta$.

Fig. 6(a)–(c) shows a density plot of the pulse amplitude relative difference $\Delta$ vs the electrical diameter $D$ for three different bead sizes (measured separately using the proposed wiring scheme,
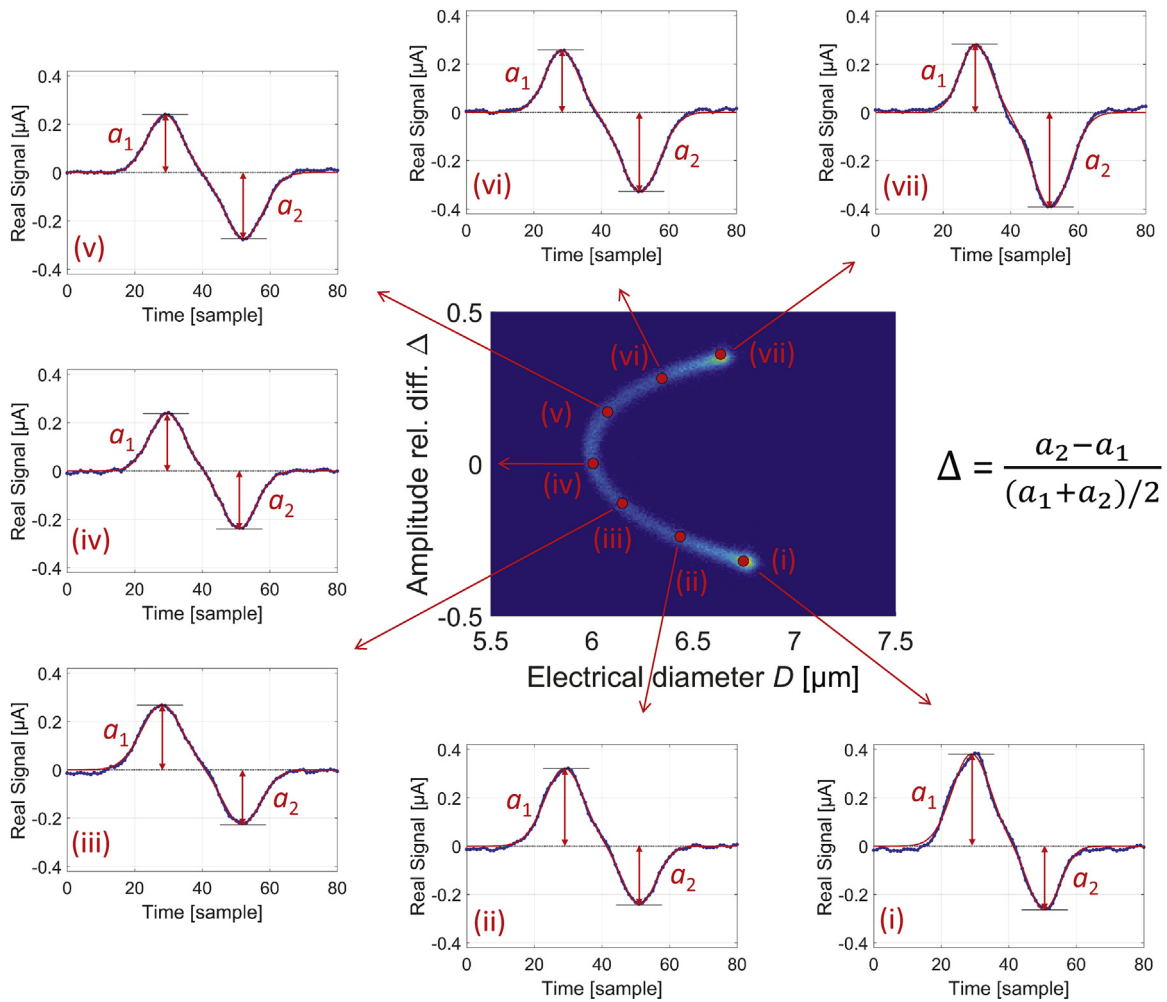
**Fig. 5.** Facing electrode chip operated using the proposed wiring scheme. Density plot for 6 μm diameter beads, with the pulse amplitude relative difference Δ plotted against the electrical diameter D. (i)–(vii) are experimental single particle signals (blue line) for the data points in the density plot. Fitting templates are also shown (red line). (For interpretation of the references to color in this figure legend, the reader is referred to the web version of the article.)
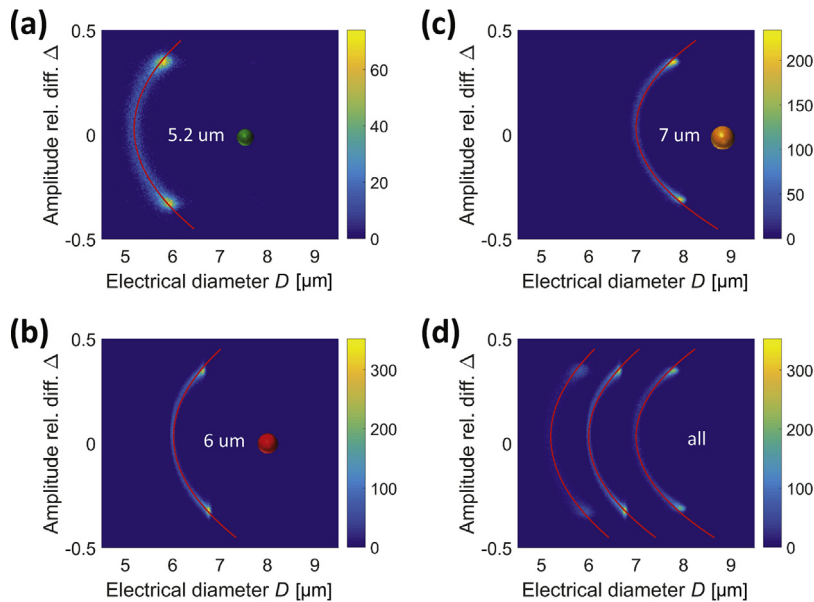
$$\Delta = \frac{a_2 - a_1}{(a_1 + a_2)/2}$$



**Fig. 6.** Facing electrode chip operated using the proposed wiring scheme. Density plot for populations of beads of different sizes, with the pulse amplitude relative difference Δ plotted against the electrical diameter D. (a) 5.2 μm diameter beads, (b) 6 μm diameter beads, (c) 7 μm diameter beads and (d) collection of the events in panels (a)–(c) plotted on the same graph. The fitted parabolas $D = a[1 + b(\Delta - c)^2]$ are shown as red lines. For each population, parameter values a, b, and c are reported in Table 1. In (d), the three parabolas are defined with a = 5.2, 6.0, 7.0 μm and the same parameters b and c (average values, Table 1). (For interpretation of the references to color in this figure legend, the reader is referred to the web version of the article.)
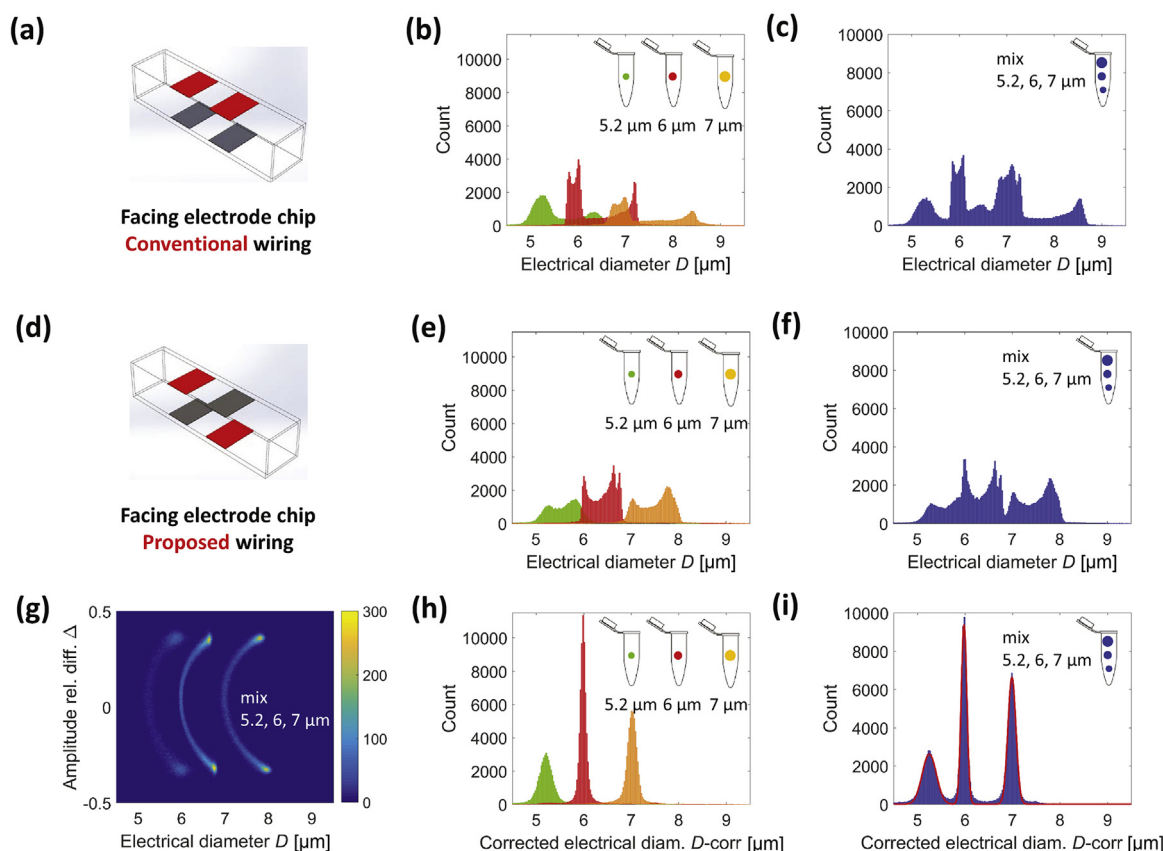
**Fig. 7.** Facing electrode chip. (a)–(c) Conventional operation mode. (a) 3D view cartoon. Histogram of the electrical diameter $D$ of 5.2, 6, and 7 μm diameter beads measured (b) separately and (c) together. (d)–(i) Proposed operation mode. (d) 3D view cartoon. (g) Density plot of the pulse amplitude relative difference $\Delta$ plotted against the electrical diameter $D$ for a mixture of 5.2, 6, and 7 μm diameter beads. (e and f) Histogram of the electrical diameter $D$ of 5.2, 6, and 7 μm diameter beads measured (e) separately and (f) together. (h and i) Histogram of the corrected electrical diameter $D$-corr, showing an almost perfect Gaussian distribution.

**Table 1**
Parameters of quadratic model equation $D = a[1 + b(\Delta - c)^2]$ used to fit data plotted in Fig. 6 (95% confidence interval within the uncertainty in the least significant digit).

| $d$ [μm] | $a$ [μm] | $b$ | $c$ |
|---|---|---|---|
| 5.2 | 5.19 | 1.06 | 0.028 |
| 6.0 | 6.02 | 0.94 | 0.032 |
| 7.0 | 7.00 | 1.04 | 0.035 |
| Mean | – | 1.01 | 0.032 |

and collected together in Fig. 6(d)). In each case the same parabolic trend is observed. This data can be fitted to a quadratic function:

$$D = a[1 + b(\Delta - c)^2], \tag{6}$$

where $a$ is particle nominal diameter, and the constants $b$ and $c$ account for the variation in signal with particle height as determined from the metric $\Delta$. These fitting parameters are listed in Table 1, and the corresponding parabolas are shown in red in Fig. 6. The constant $c$ should vanish for a channel ideally symmetric top to bottom. The fitted values are in fact very small (possibly due to minor channel asymmetry). The constants $b$ and $c$ should be independent of particle sizes, which is clear from Table 1 where the differences are minor. The mean value for constants $b$ and $c$ was then used to calculate the parabolas shown in Fig. 6(d) for the three different particle sizes, showing an excellent fit with the data. Analogous results for the coplanar electrode configuration are reported in Supplementary data, Table S1 and Figure S2.

Fig. 7(b) and (c) shows histograms of the electrical diameter $D$ obtained using the facing electrode chip and the conventional wiring scheme, relevant to individual particle populations and the mixed sample, respectively. As expected, the distribution has a significant spread and skewness, with overlap between the three populations.

Fig. 7(e) and (f) shows the analogous histograms obtained using the proposed wiring scheme. The spread and skewness are mitigated, because the cross contribution to the differential current was removed by averaging the pulse amplitudes according to Eq. (3) (cf. also Fig. 2). However, they are still present. Eq. (6) was used to correct the raw data as follows:

$$D\text{-corr} = \frac{D}{1 + b(\Delta - c)^2}, \tag{7}$$

where $b$ and $c$ are the mean values of the constants in Table 1. The corrected data is plotted in Fig. 7(h) and (i) showing an almost perfect Gaussian distribution. Fitting a Gaussian allows the coefficients of variation (CVs) to be calculated as follows: 2.82%, 0.98%, and 1.20%, for the 5.2, 6, and 7 μm diameter beads respectively. This can be compared with the manufacturers' quoted values of 2.6%, 10%,[2] and 1.7%.

Fig. 8 shows the analogous results obtained using the coplanar electrode chip. Fitting a Gaussian on the histogram of the corrected electrical diameter $D$-corr in Fig. 8(i) allows the CVs to be calculated as follows: 3.67%, 1.89%, and 1.72%, for the 5.2, 6, and 7 μm diameter beads respectively. Although somewhat greater than those provided by the facing electrode chip, reasonably low figures are obtained also using the coplanar electrode chip.

---

[2] The 6 μm diameter beads from PolySciences have a much higher reported CV than the 5.2 μm and 7 μm obtained from Sigma-Aldrich. That value is probably a conservative estimate.
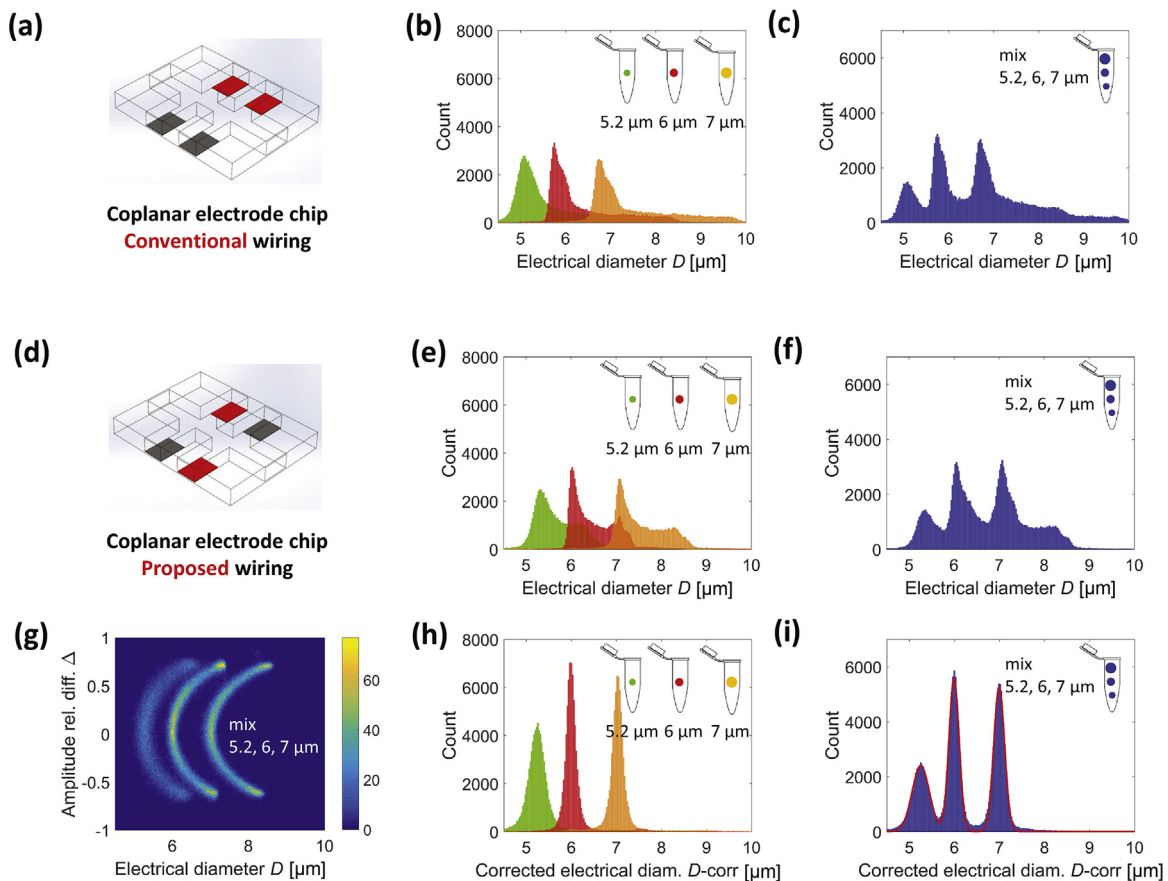
**Fig. 8.** Coplanar electrode chip. (a)–(c) Conventional operation mode. (a) 3D view cartoon. Histogram of the electrical diameter D of 5.2, 6, and 7 μm diameter beads measured (b) separately and (c) together. (d)–(i) Proposed operation mode. (d) 3D view cartoon. (g) Density plot of the pulse amplitude relative difference ∆ plotted against the electrical diameter D for a mixture of 5.2, 6, and 7 μm diameter beads. (e and f) Histogram of the electrical diameter D of 5.2, 6, and 7 μm diameter beads measured (e) separately and (f) together. (h and i) Histogram of the corrected electrical diameter D-corr, showing an almost perfect Gaussian distribution.
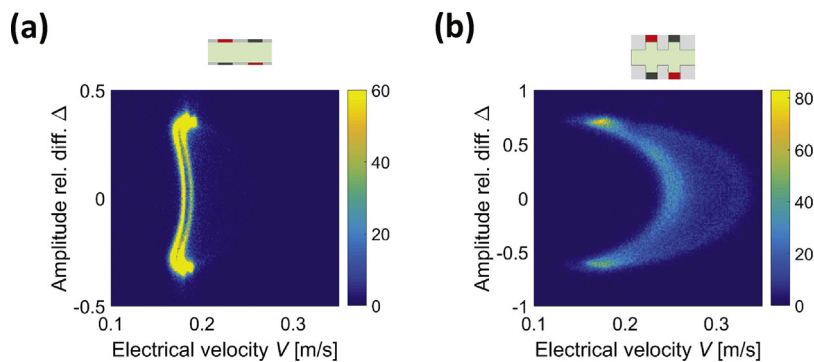


**Fig. 9.** Density plot of the pulse amplitude relative difference ∆ plotted against the electrical velocity V for the mixture of beads. (a) Facing electrode chip operated using the proposed wiring scheme: a significant level of particle focusing is observed (the density scale has been saturated, in order to make visible the parabolic profile on the right). Two profiles appear on the left, respectively relevant to 5.2 and 7 μm diameter beads obtained by Sigma–Aldrich (left profile) and 6 μm diameter beads obtained by Polysciences (right profile): cf. Fig. 10(c) and (e). (b) Coplanar electrode chip operated using the proposed wiring scheme: although some degree of focusing is apparent, many particles adopt a random distribution in the channel cross section.

Density plots of the pulse amplitude relative difference ∆ plotted against the electrical velocity V, obtained using the proposed wiring scheme, are shown in Fig. 9. The observed parabolic profiles constitute further evidence that ∆ is related to the location of the particle trajectory in the microchannel. A higher level of inertial focusing is observed when using the facing electrode chip (Fig. 9(a)) rather than the coplanar electrode chip (Fig. 9(b)). Although the channel cross sections are comparable, this is due to the different channel length (≈16 mm in the former case, ≈0.8 mm in the lat-

ter case) that particles pass through before reaching the measuring zone [18].

Density plots of the electrical velocity V plotted against the electrical diameter D are shown in Fig. 10. These plots confirm the higher level of inertial focusing observed when using the facing electrode chip (Fig. 10(a), (c), (e)) rather than the coplanar electrode chip (Fig. 10(b), (d), (f)). The new wiring scheme used with the facing electrode chip (Fig. 10(c)) supplies a narrow velocity rage, as expected when particles experience a large degree of inertial focusing. A broader velocity range is obtained using the conventional
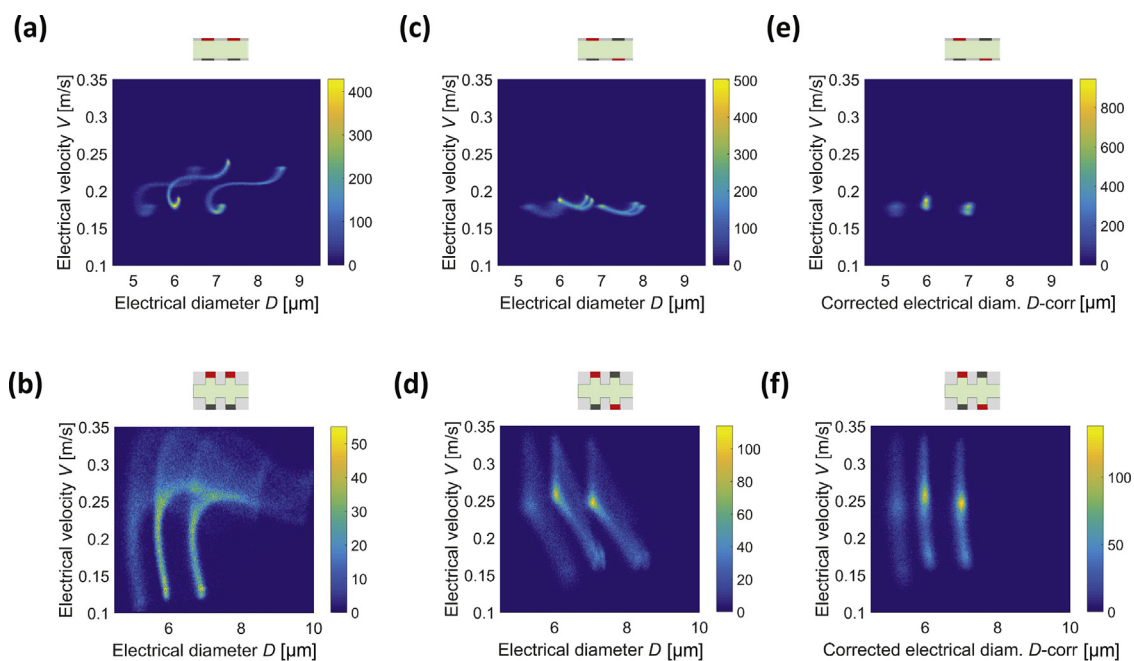
**Fig. 10.** Density plot of the electrical velocity V plotted against the electrical diameter for the mixture of beads. (a, c, and e) Facing electrode chip; (b, d, and f) coplanar electrode chip. (a and b) Conventional wiring scheme. Proposed wiring scheme, (c and d) before compensation and (e and f) after compensation.

wiring scheme (Fig. 10(a)). Comparing Fig. 10(c), (d) respectively to Fig. 10(e), (f), it appears that the simple compensation procedure in Eq. (7) enabled by the proposed wiring scheme completely eliminates the height dependent variation in electrical diameter D, i.e. all particles of a given size range have the same electrical diameter D-corr irrespective of trajectory through the channel.

## 5. Conclusions

The widely used microfluidic impedance chips comprising two pairs of electrodes are promoted to a superior level of accuracy by simply swapping two connection wires. With the novel wiring scheme, a left–right asymmetry is introduced in the system that is profitably exploited to compensate for positional dependence of the measured signals. No particle focusing mechanisms are required and the proposed operation mode successfully applies to both facing and coplanar electrode layout. The novel concept introduced in this work may open new opportunities for impedance cytometry in applications requiring accurate particle sizing and characterization.

## Author contributions

F.C and P.B. designed the research, A.D.N and L.B. took care of coplanar chip microfabrication, R.R., A.D.N. and F.C. performed experiments, F.C., P.B. and R.R. analyzed the data, F.C. wrote the paper. All authors revised the manuscript.

## Acknowledgements

## Appendix A. Supplementary data

Supplementary data associated with this article can be found, in the online version, at https://doi.org/10.1016/j.snb.2017.10.113.

## References

[1] K.C. Cheung, M. Di Berardino, G. Schade-Kampmann, M. Hebeisen, A. Pierzchalski, J. Bocsi, A. Mittag, A. Tárnok, Microfluidic impedance-based flow cytometry, Cytometry Part A 77 (7) (2010) 648–666, http://dx.doi.org/10.1002/cyto.a.20910.

[2] T. Sun, H. Morgan, Single-cell microfluidic impedance cytometry: a review, Microfluid. Nanofluid. 8 (4) (2010) 423–443, http://dx.doi.org/10.1007/s10404-010-0580-9.

[3] S. Gawad, K. Cheung, U. Seger, A. Bertsch, P. Renaud, Dielectric spectroscopy in a micromachined flow cytometer: theoretical and practical considerations, Lab Chip 4 (3) (2004) 241–251, http://dx.doi.org/10.1039/b313761a.

[4] J.-L. Hong, K.-C. Lan, L.-S. Jang, Electrical characteristics analysis of various cancer cells using a microfluidic device based on single-cell impedance measurement, Sens. Actuators B: Chem. 173 (2012) 927–934, http://dx.doi.org/10.1016/j.snb.2012.06.046.

[5] G. Mernier, W. Hasenkamp, N. Piacentini, P. Renaud, Multiple-frequency impedance measurements in continuous flow for automated evaluation of yeast cell lysis, Sens. Actuators B: Chem. 170 (2012) 2–6, http://dx.doi.org/10.1016/j.snb.2010.10.050.

[6] S.C. Bürgel, C. Escobedo, N. Haandbæk, A. Hierlemann, On-chip electroporation and impedance spectroscopy of single-cells, Sens. Actuators B: Chem. 210 (2015) 82–90, http://dx.doi.org/10.1016/j.snb.2014.12.016.

[7] I. Heidmann, G. Schade-Kampmann, J. Lambalk, M. Ottiger, M. Di Berardino, Impedance flow cytometry: a novel technique in pollen analysis, PLOS ONE 11 (11) (2016) 1–15, http://dx.doi.org/10.1371/journal.pone.0165531.

[8] K. Cheung, S. Gawad, P. Renaud, Impedance spectroscopy flow cytometry: on-chip label-free cell differentiation, Cytometry Part A 65A (2) (2005) 124–132, http://dx.doi.org/10.1002/cyto.a.20141.

[9] D. Holmes, D. Pettigrew, C.H. Reccius, J.D. Gwyer, C. van Berkel, J. Holloway, D.E. Davies, H. Morgan, Leukocyte analysis and differentiation using high speed microfluidic single cell impedance cytometry, Lab Chip 9 (20) (2009) 2881–2889, http://dx.doi.org/10.1039/B910053A.

[10] M. Evander, A.J. Ricco, J. Morser, G.T.A. Kovacs, L.L.K. Leung, L. Giovangrandi, Microfluidic impedance cytometer for platelet analysis, Lab Chip 13 (4) (2013) 722–729, http://dx.doi.org/10.1039/c2lc40896a.

[11] N. Haandbæk, S.C. Bürgel, F. Rudolf, F. Heer, A. Hierlemann, Characterization of single yeast cell phenotypes using microfluidic impedance cytometry and optical imaging, ACS Sens. 1 (8) (2016) 1020–1027, http://dx.doi.org/10.1021/acssensors.6b00286.

[12] J.S. McGrath, C. Honrado, D. Spencer, B. Horton, H.L. Bridle, H. Morgan, Analysis of parasitic protozoa at the single-cell level using microfluidic

impedance cytometry, Sci. Rep. 7 (2017), http://dx.doi.org/10.1038/s41598-017-02715-y.

[13] T. Sun, N.G. Green, S. Gawad, H. Morgan, Analytical electric field and sensitivity analysis for two microfluidic impedance cytometer designs, IET Nanobiotechnol. 1 (5) (2007) 69–79, http://dx.doi.org/10.1049/iet-nbt:20070019.

[14] D. Spencer, H. Morgan, Positional dependence of particles in microfludic impedance cytometry, Lab Chip 11 (7) (2011) 1234–1239, http://dx.doi.org/10.1039/c1lc20016j.

[15] J. Riordon, N.M. Catafard, M. Godin, Using the fringing electric field in microfluidic volume sensors to enhance sensitivity and accuracy, Appl. Phys. Lett. 101 (15) (2012) 154105, http://dx.doi.org/10.1063/1.4759033.

[16] V. Errico, A. De Ninno, F. Bertani, L. Businaro, P. Bisegna, F. Caselli, Mitigating positional dependence in coplanar electrode coulter-type microfluidic devices, Sens. Actuators B: Chem. 247 (2017) 580–586, http://dx.doi.org/10.1016/j.snb.2017.03.035.

[17] X. Mao, A. Nawaz, S. Lin, M. Lapsley, Y. Zhao, J. McCoy, W. El-Deiry, T. Huang, An integrated, multiparametric flow cytometry chip using microfluidic drifting based three-dimensional hydrodynamic focusing, Biomicrofluidics 6 (2) (2012) 024113, http://dx.doi.org/10.1063/1.3701566.

[18] D. Di Carlo, Inertial microfluidics, Lab Chip 9 (21) (2009) 3038–3046, http://dx.doi.org/10.1039/b912547g.

[19] N. Haandbæk, O. With, S.C. Bürgel, F. Heer, A. Hierlemann, Resonance-enhanced microfluidic impedance cytometer for detection of single bacteria, Lab Chip 14 (17) (2014) 3313–3324, http://dx.doi.org/10.1039/C4LC00576G.

[20] M. Shaker, L. Colella, F. Caselli, P. Bisegna, P. Renaud, An impedance-based flow micro-cytometer for single cell morphology discrimination, Lab Chip 14 (14) (2014) 2548–2555, http://dx.doi.org/10.1039/c4lc00221k.

[21] C. Grenvall, C. Antfolk, C. Bisgaard, T. Laurell, Two-dimensional acoustic particle focusing enables sheathless chip Coulter counter with planar electrode configuration, Lab Chip 14 (24) (2014) 4629–4637, http://dx.doi.org/10.1039/C4LC00982G.

[22] D. Spencer, F. Caselli, P. Bisegna, H. Morgan, High accuracy particle analysis using sheathless microfluidic impedance cytometry, Lab Chip 16 (13) (2016) 2467–2473, http://dx.doi.org/10.1039/c6lc00339g.

[23] A. De Ninno, V. Errico, F.R. Bertani, L. Businaro, P. Bisegna, F. Caselli, Coplanar electrode microfluidic chip enabling accurate sheathless impedance cytometry, Lab Chip 17 (2017) 1158–1166, http://dx.doi.org/10.1039/C6LC01516F.

[24] P. Xie, X. Cao, Z. Lin, N. Talukder, S. Emaminejad, M. Javanmard, Processing gain and noise in multi-electrode impedance cytometers: comprehensive electrical design methodology and characterization, Sens. Actuators B: Chem. 241 (2017) 672–680, http://dx.doi.org/10.1016/j.snb.2016.09.182.

[25] U. Hassan, R. Bashir, Coincidence detection of heterogeneous cell populations from whole blood with coplanar electrodes in a microfluidic impedance cytometer, Lab Chip 14 (22) (2014) 4370–4381, http://dx.doi.org/10.1039/c4lc00879k.

[26] G. Mernier, E. Duqi, P. Renaud, Characterization of a novel impedance cytometer design and its integration with lateral focusing by dielectrophoresis, Lab Chip 12 (21) (2012) 4344–4349, http://dx.doi.org/10.1039/c2lc40551b.

[27] F. Caselli, P. Bisegna, A simple and robust event-detection algorithm for single-cell impedance cytometry, IEEE Trans. Biomed. Eng. 63 (2) (2016) 415–422, http://dx.doi.org/10.1109/TBME.2015.2462292.

[28] F. Caselli, P. Bisegna, F. Maceri, EIT-inspired microfluidic cytometer for single-cell dielectric spectroscopy, J. Microelectromech. Syst. 19 (5) (2010) 1029–1040, http://dx.doi.org/10.1109/JMEMS.2010.2067204.

[29] F. Caselli, M. Shaker, L. Colella, P. Renaud, P. Bisegna, Modeling, simulation and performance evaluation of a novel microfluidic impedance cytometer for morphology-based cell discrimination, J. Microelectromech. Syst. 23 (4) (2014) 785–794, http://dx.doi.org/10.1109/JMEMS.2014.2325979.

[30] F. Caselli, R. Reale, N.A. Nodargi, P. Bisegna, Numerical investigation of a novel wiring scheme enabling simple and accurate impedance cytometry, Micromachines 8 (9) (2017) 283, http://dx.doi.org/10.3390/mi8090283.

[31] S. Gawad, L. Schild, P. Renaud, Micromachined impedance spectroscopy flow cytometer for cell analysis and particle sizing, Lab Chip 1 (1) (2001) 76–82, http://dx.doi.org/10.1039/B103933B.

[32] N. Demierre, T. Braschler, P. Linderholm, U. Seger, H. van Lintel, P. Renaud, Characterization and optimization of liquid electrodes for lateral dielectrophoresis, Lab Chip 7 (2007) 355–365, http://dx.doi.org/10.1039/B612866A.

[33] G. Mernier, N. Piacentini, R. Tornay, N. Buffi, P. Renaud, Cell viability assessment by flow cytometry using yeast as cell model, Sens. Actuators B: Chem. 154 (2) (2011) 160–163, http://dx.doi.org/10.1016/j.snb.2009.11.066.

## Biographies

**Federica Caselli** is a Researcher of Medical Engineering at the Department of Civil Engineering and Computer Science, University of Rome Tor Vergata. Her research interests include analysis and development of microdevices for biomedical use, computational biomechanics, and biomedical signal and image processing.

**Adele De Ninno** is a Postdoctoral Researcher at the Department of Civil Engineering and Computer Science, University of Rome Tor Vergata. Her research interests include microfluidics-based approaches for mimicking complex biological processes, organs-on-chip and lab-on-chip devices for point-of-care diagnostic applications.

**Riccardo Reale** is an Assistant Researcher at the Department of Civil Engineering and Computer Science, University of Rome Tor Vergata. His research interests include design, fabrication and experimental characterization of lab-on-a-chip devices for biological applications.

**Luca Businaro** is a micro and nanofabrication scientist at Institute for Photonics and Nanotechnologies, part of the Italian National Research Council. His primary scientific interest dwells in reconstituting on microfluidic chips complex biological systems such as the insult-immune system interface.

**Paolo Bisegna** is a Professor of Mechanics at the Department of Civil Engineering and Computer Science, and Director of the Medical Engineering Program, University of Rome Tor Vergata. His research interests include biomedical microdevices, biomechanics and computational mechanics.